

Original Research

M6A Methyltransferase METTL3 Modulates Traumatic Brain Injury by Targeting Ferroptosis

Fei Qin¹, Fan Li², Wenxiao Zhao³, Suqin Zhang¹, Jiang Shen³, Xinyu Yang^{1,*}

Academic Editor: Thomas Heinbockel

Submitted: 21 November 2024 Revised: 19 February 2025 Accepted: 24 February 2025 Published: 24 April 2025

Abstract

Background: Traumatic brain injury (TBI) is a disease caused by external forces that damage brain structure and function. After TBI, iron accumulation and reactive oxygen species (ROS) increase lipid peroxidation, promoting ferroptosis. Methyltransferase-like 3 (METTL3) inhibits ferroptosis by modulating related signaling pathways. This study investigates the effects of METTL3 on neuronal ferroptosis in TBI, offering new insights and potential therapies. Methods: TBI mouse and neuron cell models were established and treated with METTL3 overexpression. The Morris Water Maze (MWM) test evaluated cognitive function. Histological staining of brain tissues was conducted to assess brain injury, nuclear pyknosis, and iron accumulation. The activation of neurons, microglia, and astrocytes were detected using immunofluorescence staining. Neuron cell proliferation was measured using the Cell Counting Kit 8 (CCK-8). Quantitative PCR (qPCR) and western blot detected the mRNA and protein expression. Ferroptosis was assessed by measuring the accumulation of iron, malondialdehyde (MDA), superoxide dismutase (SOD), and ROS. The quantification of the N6-methyladenosine (m6A) RNA methylation levels in cells was quantified using the m6A-ELISA assay. Methylated RNA immunoprecipitation (MeRIP) assays were conducted to analyze the m6A modification on GPX4 mRNA. The interaction between YTHDF2 and GPX4 mRNA was measured using RNA pulldown and RNA immunoprecipitation (RIP) assays. Results: METTL3 expression was downregulated in TBI-injured brain tissues. Overexpression of METTL3 improved cognitive function and brain recovery while simultaneously reducing ferroptosis and neuroinflammation. METTL3 overexpression upregulated GPX4 expression both in vitro and in vivo. Further studies indicated that m6A reader protein YTHDF2 binds to GPX4 mRNA, consequently mediating the METTL3-regulated m6A enrichment and RNA stability of GPX4. Knockdown of GPX4 and treatment with ferroptosis inducer abolished the protective effects of METTL3 on neurons. Conclusion: METTL3 exhibits anti-ferroptosis properties and promotes brain injury recovery after TBI by regulating the m6A modification and RNA stability of GPX4.

Keywords: traumatic brain injury; ferroptosis; m6a modification; epigenetic regulation; METTL3

1. Introduction

Traumatic brain injury (TBI) is a significant global health issue that leads to substantial morbidity, mortality, and economic costs worldwide, with over 50 million new cases occurring annually [1]. Despite the high burden of severe TBI, no effective pharmacological intervention or treatment has been identified for TBI patients in randomized controlled trials, indicating that the key mechanisms leading to cell death and functional deficits after TBI remain elusive [2]. In the pathophysiological process of TBI, various forms of cell death occur, including apoptosis, necrosis, autophagy, pyroptosis, and ferroptosis [3–5]. However, the mechanisms of ferroptosis in the context of TBI have not been extensively explored.

Ferroptosis is a recently identified form of regulated cell death that is dependent on iron and lipid peroxidation products [6]. It is implicated in a variety of brain diseases and injuries, including ischemic stroke, intracerebral hemorrhage, and TBI [7–9]. The dysregulation of key com-

ponents of the ferroptosis mechanism includes iron homeostasis, glutathione (GSH) depletion, and lipid peroxidation [10]. Research demonstrates that alterations in phosphatidylethanolamine oxidation, protein expression, and GSH levels following TBI are indicative of ferroptosis activation. Transmission electron microscopy further corroborates these findings by revealing characteristic features of ferroptosis, such as mitochondrial shrinkage. Moreover, studies have shown that inhibiting ferroptosis can potentially improve the long-term prognosis of TBI patients, underscoring the significant role of ferroptosis in the progression and outcome of TBI [11–13].

Traditionally, epigenetic regulation refers to the chemical modifications of DNA or histones, which can regulate gene expression independently of changes in the genomic sequence [14,15]. Dysregulation of enzymes involved in epigenetic modifications has profound implications for human diseases and is frequently reported in various types of cancer [16,17]. Similarly, RNA

¹Department of Neurosurgery, Tianjin Medical University General Hospital, 300052 Tianjin, China

²Department of Neurosurgery, Heji Hospital Affiliated to Changzhi Medical College, 046011 Changzhi, Shanxi, China

 $^{^3}$ Department of Neurosurgery, Gaoping People's Hospital, 048400 Gaoping, Shanxi, China

^{*}Correspondence: yangxinyu@tmu.edu.cn (Xinyu Yang)

also carries hundreds of different sites for various posttranscriptional modifications. N6-methyladenosine (m6A) is the most prevalent mRNA modification in eukaryotic cells [18]. Methyltransferase-like 3 (METTL3) is the principal "writer" that introduces m6A methylation to RNA. YTHDF2, an m6A "reader", recognizes and binds to these modifications [19]. METTL3 and YTHDF2 frequently collaborate to modulate the levels of m6A modifications in RNA. In glioma, YTHDF2 promotes UBXN1 degradation by recognizing METTL3-catalyzed m6A modifications, thereby activating the NF-kB pathway and accelerating glioma progression [20]. In liver cancer, METTL3 suppresses SOCS2 expression via a YTHDF2-dependent posttranscriptional mechanism, promoting hepatocarcinogenesis [21]. GPX4 is a critical enzyme that clears lipid peroxides. GPX4 dysfunction causes mitochondrial contraction, reactive oxygen species (ROS) accumulation, and increased lipid peroxide levels. Studies show that METTL3 inhibits ferroptosis by maintaining GPX4 expression at the translational level. METTL3 also regulates GPX4 to prevent ferroptotic signaling, which affects diseases such as glioblastoma, asthma, and aortic dissection [22–24].

A recent study has shown that *METTL3* protein expression is increased in inflammatory microglia in human and mouse TBI models. Selective knockout of *METTL3* has been shown to inhibit microglial pathogenic activity and enhance functional recovery post-TBI [25], yet the underlying regulatory roles and molecular mechanisms remain elusive. In this study, we aimed to explore the role of *METTL3* in ferroptosis during TBI and to investigate the molecular mechanisms.

2. Materials and Methods

2.1 Mouse TBI Model

Animal experiments were conducted in accordance with the guidelines of the Animal Ethic Committee of Medical Discovery Leader (MDL, Approval number: MDL2023-08-26-01). Eight-week-old male C57BL/6J mice (wild-type, $METTL3^{+/+}$, and $METTL3^{+/+}GPX4^{-/-}$), weighing between 20 and 25 grams, were purchased from Cyagen Biotechnology Co., Ltd. (Suzhou, China). A total of 60 mice were used in the experiment. The mice were placed in a temperature-controlled room (23 \pm 2 °C) with a controlled lighting schedule.

Before surgery, the mice were assigned codes and evenly distributed into the following groups: sham, TBI model, model+NC, model+METTL3, model+METTL3+siGPX4, model+METTL3+erastin groups (10 mice in each group). Mouse TBI models were created through a controlled cortical impact (CCI) procedure [26]. The mice were positioned face-down in a stereotaxic frame. A surgical incision was made to expose the skull, and a 3 mm craniotomy was performed on the left side, positioned roughly halfway between the bregma

and lambda, lateral to the midline. The skull flap was meticulously removed without damaging the underlying dura mater. The CCI was inflicted perpendicularly to the brain surface using a pneumatic cortical impactor (AmScien Instruments, Richmond, VA, USA). The settings for the impactor were as follows: an impact pressure of 10 KPa, a depth of 1.0 mm, and a duration of 70 milliseconds. The craniotomy site was immediately sutured shut using standard surgical materials after TBI. Mice in the sham group underwent all surgical steps except for the actual CCI. For the model+METTL3+erastin groups, the mice were intraperitoneally administrated with erastin (329600, Sigma-Aldrich, St. Louis, MO, USA) at a dose of 20 mg/kg body weight, 1 h after TBI. To ensure consistency and reduce variability, the surgical procedures, drug administrations, and CCI operations were conducted by the same experienced personnel. All surgical interventions were performed under deep anesthesia induced by intraperitoneal injection of sodium pentobarbital (1% w/v in sterile saline, 50 mg/kg body weight). Anesthesia depth was confirmed by the absence of corneal reflex and negative response to the toe pinch test.

2.2 Behavioral Analysis

To assess the efficacy of the interventional treatments, the Morris Water Maze (MWM) test was performed 7 days post-TBI. Prior to the TBI, mice underwent a 3-day training period to acclimate to locating a submerged platform in the maze, with three attempts per day, each limited to 90 seconds. Mice unable to find the platform within this period were guided to it and remained there for 15 seconds to familiarize themselves with the location. A probe trial, conducted 24 hours after training, tracked the latency to first reach the platform and the frequency of traversing its former location. These metrics were recorded and analyzed using a computer-assisted video tracking system (EthoVision XT 16.0, Noldus Information Technology, Wageningen, Netherlands), providing precise records of the swimming paths and times.

2.3 Neurological Severity Score Assessment

Neurological severity score (NSS) was used to evaluate motor, balance, and reflex functions in mice post-TBI, offering a comprehensive assessment of neurological status [27]. Trained professionals conducted NSS assessments, ensuring accuracy and consistency through specialized training. The NSS ranges from 0 to 10, with increasing scores signifying more pronounced neurological deficits. The grading system is as follows: 0–3 points indicate nearly normal neurological function or mild deficits; 4–6 points suggest moderate deficits; and 7–10 points represent severe impairments.



2.4 Brain Sections Preparation

After the completion of the experimental treatments, the mice were anesthetized using an intraperitoneal injection of sodium pentobarbital (1.0% w/v in normal saline, 50 mg/kg body weight) to ensure minimal distress. The anesthetized mice were then euthanized by cervical dislocation. Subsequently, the brain tissues were carefully excised and immediately placed in a chilled phosphate-buffered saline (PBS) solution to prevent degradation. Brain tissues were fixed in 4% paraformaldehyde for 24 hours at 4 °C, dehydrated through a 90% ethanol solution, and then cleared in xylene. The tissues were sectioned into 5- μ m-thick slices using a microtome.

2.5 Crystal Violet Staining

Brain tissue sections were stained with 0.1% crystal violet solution (C0121, Beyotime, Shanghai, China) for 30 minutes, then quickly rinsed with PBS to remove excess stain. Subsequent dehydration with 95% and 100% ethanol for 5 minutes each, followed by clearing with xylene for 5 minutes (repeated twice), preceded mounting with a neutral medium. The stained sections were examined under a Nikon TE300 microscope (Nikon, Tokyo, Japan).

2.6 Nissl Staining

Brain tissue sections were immersed in Nissl staining solution (C0117, Beyotime, Shanghai, China) for 5 minutes at room temperature. After staining, the sections were rinsed with distilled water for 5 minutes. The stained sections were examined under a light microscope (Nikon, Tokyo, Japan) to visualize the morphology of neuron cells.

2.7 Fluoro-Jade B (FJB) Staining

To identify degenerating neurons, FJB staining was performed on the brain sections according to the manufacturer's protocol (AG310, Millipore, Darmstadt, Germany). The sections were first incubated in a 0.06% potassium permanganate solution for 10 minutes, washed with distilled water for 2 minutes, and stained with a 0.0004% solution of Fluoro-Jade B for 30 minutes. The stained sections were examined using a Nikon TE300 microscope to visualize degenerative neurons. The stained sections were examined under a Nikon TE300 fluorescence microscope equipped with filters to visualize degenerating neurons.

2.8 Perls' Prussian Blue Staining

To identify iron deposition within cellular structures, Perls' Prussian blue staining was performed using the Prussian Blue Iron Stain Kit (G1422, Solarbio, Beijing, China). Brain sections were immersed in the Perls Stain Solution for 30 minutes and rinsed with distilled water for 5 minutes. Subsequently, the sections were dehydrated with anhydrous ethanol for three times, each for 5 minutes, followed by clearing in dimethylbenzene for 5 minutes. The sections were then removed, and neutral resin was applied

dropwise for mounting. Iron deposits were visualized as blue particles within cellular structures using a light microscope. These deposits were quantified with ImageJ software (version 1.53; National Institutes of Health, Bethesda, MD, USA).

2.9 Immunohistochemical and Immunofluorescence Staining

Brain slices were rehydrated with PBS for 10 minutes and then blocked with a buffer consisting of 0.3% Triton X-100 and 10% BSA in PBS for 1 hour to reduce non-specific binding. The sections were incubated overnight at 4 °C with primary antibodies targeting GPX4 (ab125066, 1:250, Abcam, Cambridge, UK), SLC7A11 (ab307601, 1:500, Abcam), METTL3 (ab195352, Abcam), NeuN (ab104224, 1:3000, Abcam), GFAP (ab7260, 1:5000, Abcam), and Iba-1 (ab178846, 1:2000, Abcam). After washing with PBS, the sections were incubated with secondary antibodies for 1 hour at room temperature: Antirabbit IgG H&L (ab205718, 1:1000, Abcam) for GPX4, SLC7A11, METTL3, and GFAP; Anti-mouse IgG H&L (ab205719, 1:1000, Abcam) for NeuN; and Anti-goat IgG H&L (ab205720, 1:1000, Abcam) for Iba-1. For immunofluorescence staining, sections were mounted with a solution containing 4',6-diamidino-2-phenylindole (DAPI, 62248, Thermo Scientific, Rockford, IL, USA) to stain cell nuclei. The slides were examined under a fluorescence microscope (Leica, Wetzlar, Germany) to visualize cell density and specific protein expression within the brain tissue.

2.10 Detection of Ferroptosis

The levels of total iron and ferrous irons in the ipsilateral cortex were assessed using an iron assay kit (ab83366, Abcam, Cambridge, UK). Malondialdehyde (MDA), superoxide dismutase (SOD) and ROS levels in cortex tissues were measured using the lipid peroxidation MDA assay kit (S0131S, Beyotime, Shanghai, China), Total SOD detection kit (S0101M, Beyotime, Shanghai, China) and Tissue ROS test kit (BB-460512, Bestbio, Shanghai, China), respectively.

2.11 Cell Culture and In Vitro Model

Mouse primary cortical neurons were extracted from E15.5 mouse embryos as previously described [28], and the mouse hippocampal neuronal cell line HT-22 was from the Wanwu Biotechnology Co., Ltd. (Hefei, China). Primary cortical neurons exhibited a clear cell body with multiple long, slender processes extending from the soma, while HT-22 cells displayed typical neuronal-like morphology with elongated cell bodies and processes. Both primary neurons and HT-22 cells were cultured in DMEM (Gibco, New York, NY, USA) supplemented with 10% fetal bovine serum (Gibco, USA), 1% streptomycin, and penicillin mix at 37 °C with 5% CO₂. To ensure cell purity and authenticity, mycoplasma detection and short tandem repeat (STR)



profiling were conducted. No mycoplasma contamination was detected in any of the cell cultures.

To overexpress METTL3 and YTHDF2, mouse METTL3 (NM 019721.2) and YTHDF2 (NM 145393.4) were synthesized and cloned into the pLVX plasmid vector (General Biosystems, Anhui, China) and the complete plasmid sequence have been provided in Supplementary Fig. The siRNA targeting 1. METTL3 (5'-UCUAUCUCCAGAUCAACAUCG-3'; 5'-GCUACAAUCACAUCGCAGUCC-3'; GAUAUCACAACAGAUCCACUG-3'), siRNA targeting (5'-UAGUAACUGGGUAAGUAGGAG-YTHDF2 5'-UGGUUUAUUCUCGUUGUUCUC-3'; UUUGAAAUCAAAUUAAUCCUG-3'), siRNA targeting GPX4 (5'-AGUUUACGUCAGUUUUGCCUC-3') and nonsense siRNA (5'-UUCUCCGAACGUGUCACGU-3') were constructed by RiboBio (Guangzhou, China). Cells were transfected for 24 hours, after which a mechanical scratch injury was created using a 200 µL pipette tip to establish the cell injury model. Transfections were performed using Lipofectamine 2000 (Invitrogen, Carlsbad, CA, USA).

2.12 Cell Viability Assays

Cell viability was assessed by the Cell Counting Kit-8 (C0038, Beyotime, Shanghai, China). Briefly, cells were harvested and resuspended in complete culture medium to prepare a cell suspension with a density of 2×10^4 cells/mL. A volume of 100 µL of the cell suspension, containing 2000 cells, was added to each well of a 96-well plate. After the incubation period, 10 µL of Cell Counting Kit 8 (CCK-8) solution was added to each well, and the plate was gently mixed to ensure even distribution of the reagent. The cells were then incubated for 1 hour at 37 °C in a humidified atmosphere with 5% CO₂. The absorbance of each well was measured at a wavelength of 450 nm using a Microplate Reader (800TSUV, BioTek, Winooski, VT, USA). The cell viability rate was calculated by comparing the absorbance values of the experimental groups with those of the control group.

2.13 Western Blotting Assay

The samples were homogenized in lysis buffer (P0023, Beyotime, Shanghai, China) and sonicated. The homogenate was then centrifuged at 4 °C for 20 minutes at 12,000 g to separate soluble proteins. Protein concentrations were measured using a BCA kit (P0009, Beyotime, Shanghai, China). Proteins were resolved on SDS-PAGE gels ranging from 7.5% to 12.5% (Bio-Rad, Hercules, CA, USA) and transferred onto polyvinylidene fluoride membranes (Millipore, Darmstadt, Germany), and incubated overnight at 4 °C with primary antibodies against SLC7A11 (ab307601, 1:1000, Abcam, Cambridge, UK), IL-6 (ab290735, 1:1000, Abcam), TNF- α (ab183218, 1:2000, Abcam), IL-1 β (ab315084, 1:1000, Abcam), GPX4

(ab125066, 1:2000, Abcam), METTL3 (ab195352, 1:1000, Abcam), YTHDF2 (ab220163, 1:1000, Abcam), and β -actin (AF7018, 1:3000, Affinity, Cincinnati, OH, USA). The next day, membranes were incubated with secondary antibodies (ab97051, 1:2000, Abcam) for 1.5 hours at room temperature. Immunoreactive protein bands were visualized using an enhanced chemiluminescence system (Thermo, USA), and band intensities were quantified using ImageJ software (version 1.53, National Institutes of Health, USA).

2.14 Quantitative PCR (qPCR) Assay

Total RNA was extracted from the samples using TRIzol reagent (15596018CN, Invitrogen, CA, USA), and quantified using a NanoDrop 2000C spectrophotometer (Thermo, USA). Reverse transcription was performed using PrimeScriptTM RT Master Mix (RR036A, Takara, Japan) to generate cDNA. qPCR reactions were conducted using a SYBR Green master mix (04913850001, Roche, Basel, Switzerland) to ensure accuracy. mRNA levels were normalized to the housekeeping gene β -actin as an endogenous control, and relative quantification was calculated using the comparative cycle threshold (Ct) method. Primer sequences used are as follows:

GPX4-F: 5'-TGGTTTACGAATCCTGGCCT-3', *GPX4*-R: 5'-GGCATCGTCCCCATTTACAC-3';

SLC7A11-F: 5'-GTCTGCCTGTGGAGTACTGT-3', *SLC7A11*-R: 5'-ATTACGAGCAGTTCCACCCA-3';

METTL3-F: 5'-TGGCCTCTTCAGCATCAGAA-3', *METTL3*-R: 5'-ACTGACCTTCTTGCTCTGCT-3';

YTHDF2-F: 5'-TGCTTGGTCTACTGGAGGTG-3', *YTHDF2*-R: 5'-AATGGAGTGCTACCTAGGGC-3';

*IL-6-*F: 5'-ACTTCCATCCAGTTGCC-3', *IL-6-*R: 5'-ATGTGTAATTAAGCCTCCGAC-3';

TNF- α -F: 5'-ACGGCATGGATCTCAAAGACAAC-3', *TNF*- α -R: 5'-AGATAGCAAATCGGCTGACGG-3';

IL- $I\beta$ -F: 5'-TTGAAGTTGACGGACCCCAA-3', IL- $I\beta$ -R: 5'-CCACAGCCACAATGAGTGA-3';

 β -actin-F: 5'-CTCCTGAGCGCAAGTACTCT-3', β -actin-R: 5'-TACTCCTGCTTGCTGATCCAC-3'.

2.15 Enzyme Linked Immunosorbent Assay (ELISA)

The production of inflammatory factors IL-6 (ab222503, Abcam, Cambridge, UK), TNF- α (ab208348, Abcam), and IL-1 β (PI301, Beyotime, Shanghai, China) was measured by using ELISA kits. Absorbance was measured at 450 nm using a microplate reader (Varioskan LUX, Thermo, USA). The concentrations of the inflammatory factors were determined by comparing the absorbance values to a standard curve generated using known concentrations of recombinant proteins.

2.16 M6A Quantification (m6A-ELISA Assay)

The level of m6A RNA methylation in cells was quantified using an m6A RNA Methylation Quantification Kit



(ab185912, Abcam, Cambridge, UK). In brief, mRNA was extracted and bound to a strip well for 90 minutes. After washing, captured, detection, and enhancer antibodies were added sequentially. The color-developing solution was then added, and the absorbance was measured at 450 nm using a microplate reader.

2.17 Immunoprecipitation (MeRIP) Assay

The MeRIP assay was performed using the Magna MeRIP m6A Kit (17-10499, Millipore, Darmstadt, Germany) to analyze the m6A modification in RNA samples. The enrichment of *GPX4* mRNA was measured by qPCR.

2.18 RNA Pulldown

The interaction between *YTHDF2* and *GPX4* mRNA was measured by PierceTM Magnetic RNA-Protein Pull-Down Kit (PI20164, Thermo, USA), which contains streptavidin-coated magnetic beads (1 μm diameter, silica core, binding capacity: 1 μg biotinylated probe per 1 mg beads). In brief, the biotin-labeled GPX4-specific probe was reacted with magnetic beads, which were then mixed with protein lysate samples. After washing and elution, *YTHDF* pulled down by *GPX4* mRNA was detected by western blot.

2.19 RIP Assay

The RIP assay was performed using antibodies against YTHDF2 or a negative IgG control with Magna RIPTM RNA-Binding Protein Immunoprecipitation Kit (17-700, Millipore, Darmstadt, Germany). Protein A/G-coated magnetic beads (1 μm diameter, agarose matrix, provided in the kit) were pre-washed with RIP wash buffer and incubated with 5 μg of anti-YTHDF2 antibody or negative control IgG (19145, Sigma-Aldrich, St. Louis, USA) for 1 hour at 4 °C. Cells were lysed in RIP lysis buffer, and the lysates were incubated with RIP immunoprecipitation buffer containing immunoprecipitated with A/G magnetic beads. The magnetic frame was used to fix bead-bound complexes and wash away unbound material. RNA was extracted from the bead-bound complexes, and *GPX4* mRNA levels were analyzed by qPCR.

2.20 GPX4 mRNA Degradation Assay

Cells transfected with siMETTL3, siYTHDF2, or siNC were treated with actinomycin D for 0, 3, and 6 h. RNA was extracted, and *GPX4* mRNA levels were measured by qPCR.

2.21 Statistical Analysis

Statistical analyses were conducted using GraphPad Prism 9 (San Diego, CA, USA). Comparisons between two groups were analyzed using Student's *t*-test, while multiple groups were analyzed by one-way ANOVA followed by Tukey's post hoc test. Statistical significance was de-

fined as p < 0.05. Data are presented as mean \pm standard deviation (SD) unless otherwise noted.

3. Results

3.1 METTL3 is Downregulated during TBI-Induced Brain Damage

We established a mouse model of TBI to investigate the ferroptosis. MWM test was employed to assess cognitive function in mice. Compared to the sham group, TBI resulted in increased path lengths (Fig. 1A) and a decreased number of dentate gyrus neurons (Fig. 1B). Brain tissue images and the NSS confirmed the successful creation of the TBI model (Fig. 1C,D). Histological analyses, including HE, Nissl, Perls, FJB staining, and immunofluorescence, revealed significant brain injury (Fig. 1E), cytoplasmic shrinkage or nuclear pyknosis (Fig. 1F), iron-positive cells (Fig. 1G, Supplementary Fig. 2), and degeneration of cortical neurons (Fig. 1H, Supplementary Fig. 2) in TBI tissues, along with reduced expression of the neuronal marker NeuN (Fig. 1I, Supplementary Fig. 2). Additionally, TBI tissues exhibited significantly elevated levels of MDA, Fe²⁺, total iron, and lipid ROS, along with significantly decreased SOD levels (Fig. 1J, p < 0.05), indicative of ferroptosis. Correspondingly, protein and mRNA levels of the ferroptosis-suppressing factors GPX4 and SLC7A11 were reduced in TBI mice brain tissues (Fig. 1K,L, p <0.05). Immunofluorescence staining further revealed significantly diminished fluorescence intensity for GPX4 and SLC7A11 in the TBI group compared to the sham group (Fig. 1M, Supplementary Fig. 3, p < 0.05). Screening of m6A modulators in TBI tissues identified METTL3, an m6A writer, as significantly downregulated at the mRNA level (Fig. 1N, p < 0.05). This decrease in METTL3 expression was further confirmed by western blot and immunofluorescence (Fig. 10,P, Supplementary Fig. 3, p <0.05). These findings suggest that METTL3 may play a role in regulating ferroptosis during TBI.

3.2 Overexpression of METTL3 Mitigates TBI-Induced Damage and Ferroptosis

To assess the impact of *METTL3* on TBI progression, we administered METTL3 overexpression in the TBI model.

qPCR and western blot analyses confirmed that this treatment successfully restored the mRNA and protein levels of *METTL3* in TBI-damaged brain tissues (Fig. 2A–C, **Supplementary Fig. 4**, p < 0.05). Notably, *METTL3* overexpression enhanced cognitive function (Fig. 2D) and reduced brain damage induced by TBI (Fig. 2E–G, p < 0.05). Histological staining of cortex tissues revealed that *METTL3* overexpression alleviated the brain injury (Fig. 2H), nuclear pyknosis (Fig. 2I), presence of ironpositive cells (Fig. 2J, **Supplementary Fig. 5**), and degeneration of cortical neurons (Fig. 2K, **Supplementary Fig. 5**), while also increasing NeuN-positive cells (Fig. 2L, **Sup**



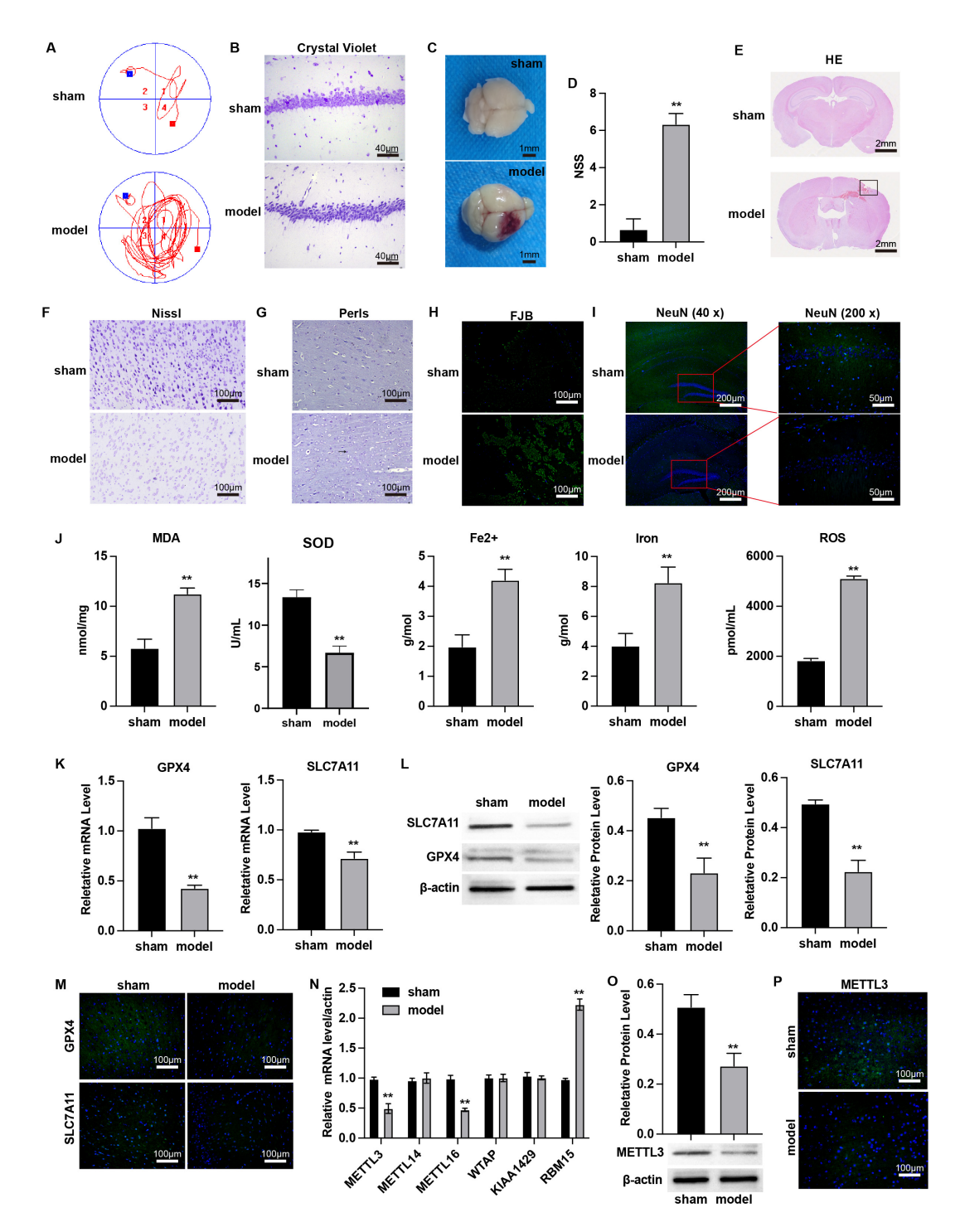


Fig. 1. Downregulation of *METTL3* in **TBI-induced brain injury.** (A) The Morris Water Maze (MWM) test was performed on day 7 post-TBI. (B) Crystal violet staining of brain tissues. Scale bar = 40 μm. (C) Brain representative images. Scale bar = 1 mm. (D) Neurological severity score (NSS) scores indicating brain tissue damage. (E–I) Representative images of (E) HE, scale bar = 2 mm, (F) Nissl, scale bar = 100 μm, (G) Perls (arrows indicate iron-positive cells), Scale bar = 100 μm, (H) Fluoro-Jade B (FJB), scale bar = 100 μm, and (I) immunofluorescence staining of markers of neuron (NeuN) in brain sections, scale bar = 200 μm or 50 μm; cortical contusion areas are represented by rectangles. (J) The cortical levels of MDA, SOD, Fe²⁺, total iron, and lipid ROS were measured. (K–M) The mRNA and protein levels of *GPX4* and *SLC7A11* in cortex tissues of TBI mice were measured by (K) qPCR, (L) western blot, and (M) immunofluorescence staining, scale bar = 100 μm. (N) The mRNA levels of m6A modification regulators in cortex tissues were measured by qPCR assay. (O,P) The protein level of METTL3 in cortex tissues was detected by (O) western blot and (P) immunofluorescence staining. Scale bar = 100 μm. **p < 0.01. n = 3 for each group. TBI, traumatic brain injury; MDA, malondialdehyde; SOD, superoxide dismutase; ROS, reactive oxygen species; m6A, N6-methyladenosine; qPCR, Quantitative PCR.

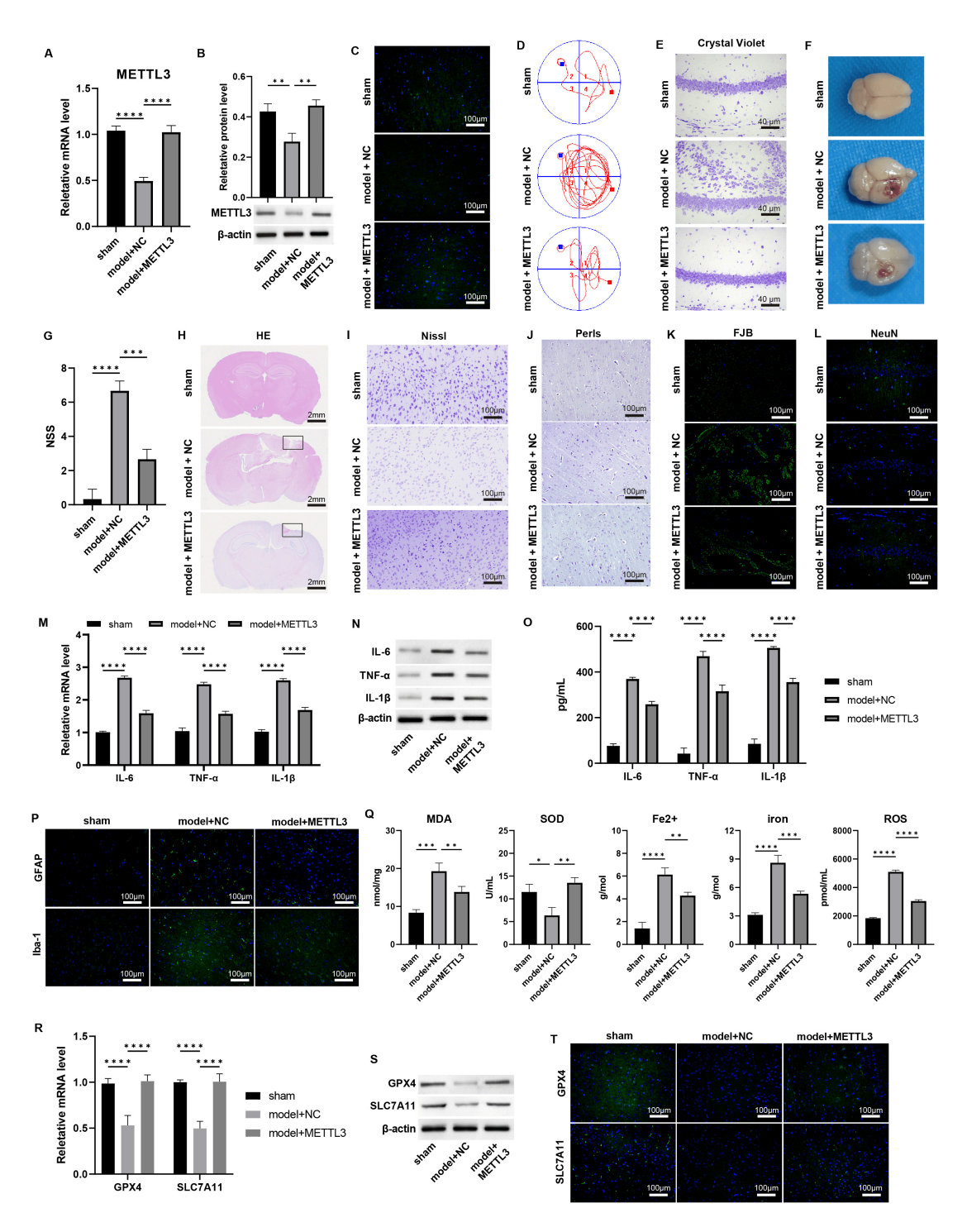


Fig. 2. Overexpression of *METTL3* **alleviates the TBI damages and ferroptosis.** (A–C) The mRNA and protein levels of METTL3 in mouse brain tissues were measured by (A) qPCR, (B) western blot, and (C) immunofluorescence staining. Scale bar = 100 μm. (D) The Morris Water Maze (MWM) test was performed on day 7 post-TBI. (E) Crystal violet staining of brain tissues. Scale bar = 40 μm. (F) Representative images of the brain. (G) NSS scoring of brain tissue damage. (H–L) Representative images of (H) HE, scale bar = 2 mm, (I) Nissl, scale bar = 100 μm. (J) Perls, scale bar = 100 μm. (K) Fluoro-Jade B (FJB), scale bar = 100 μm, and (L) immunofluorescence staining of markers of neuron (NeuN) in brain sections, scale bar = 100 μm; Cortical contusion areas are represented by rectangles. (M–O) The mRNA and protein levels of IL-6, TNF- α , and IL-1 β in cortex tissues of TBI mice were measured by (M) qPCR, (N) western blot, and (O) ELISA experiment. (P) Immunofluorescence staining of GFAP and Iba-1. Scale bar = 100 μm. (Q) The cortical levels of MDA, SOD, Fe²⁺, total iron, and lipid ROS were measured. (R–T) The mRNA and protein levels of *GPX4* and *SLC7A11* in cortex tissues of TBI mice were measured by (R) qPCR, (S) western blot, and (T) immunofluorescence staining. Scale bar = 100 μm. *p < 0.05, **p < 0.01, ***p < 0.001, ****p < 0.001, ****p < 0.0001, n = 3 for each group.

plementary Fig. 5). Moreover, METTL3 overexpression reduced the production and secretion of inflammatory factors *IL*-6, *TNF*- α , and *IL*-1 β (Fig. 2M–O, **Supplementary Fig. 6**, p < 0.05) and inhibited the activation of Iba-1+ microglia and GFAP+ astrocytes during TBI (Fig. 2P, **Supplementary Fig. 7**). Furthermore, *METTL3* treatment reduced ferroptosis biomarkers, including the MDA, Fe²⁺, total iron, and lipid ROS, upregulated SOD levels (Fig. 2Q, p < 0.05), and concurrently promoted the transcription and expression of *GPX4* and *SLC7A11* (Fig. 2R–T, **Supplementary Figs. 7**, 8, p < 0.05).

3.3 METTL3 Overexpression Enhances Neuronal Viability and Inhibits Ferroptosis In Vitro

To investigate the protective role of METTL3 on neurons in vitro, we first isolated mouse primary cortical neurons, which expressed the neuronal marker NeuN (Supplementary Fig. 9) and subsequently established a cellular model to simulate mechanical injury akin to that experienced during TBI. We treated these cells with METTL3 overexpression. The downregulation of METTL3 observed in damaged neurons was effectively reversed by its overexpression (Fig. 3A,B, p < 0.05). Notably, *METTL3* overexpression significantly enhanced neuronal viability (Fig. 3C, p < 0.05) and mitigated ferroptosis triggered by mechanical stress (Fig. 3D,E, p < 0.05). Furthermore, while the transcription and expression levels of GPX4 and SLC7A11 were diminished in mechanically damaged neurons, METTL3 overexpression restored these levels (Fig. 3F-K, Supplementary Fig. 10, p < 0.05), indicating a suppressive effect on ferroptosis.

3.4 METTL3 Epigenetically Regulates GPX4 Expression in Neurons

To explore the underlying mechanisms of METTL3mediated neuronal functions, we conducted a knockdown of METTL3 in primary neurons and HT-22 cells, selecting siMETTL3-1 for further analysis (Fig. 4A,B, p < 0.05). The knockdown of METTL3 led to a decrease in total m6A levels on RNA (Fig. 4C, p < 0.05) and reduced m6A enrichment on GPX4 mRNA (Fig. 4D, p < 0.05). Additionally, METTL3 depletion resulted in enhanced GPX4 RNA degradation in neurons and HT-22 cells (Fig. 4E, p < 0.05). YTHDF2 was found to bind to GPX4 mRNA as demonstrated by RNA pulldown assays (Fig. 4F), suggesting its role in METTL3-mediated regulation of GPX4 m6A modification and stability. We further depleted YTHDF2 using siRNAs to elucidate the METTL3/YTHDF2 axis in neurons. siYTHDF2-1 effectively downregulated YTHDF2 mRNA and protein expression (Fig. 4G,H, Supplementary Figs. 11,12, p < 0.05). RIP assays showed that METTL3 knockdown decreased YTHDF2 binding to GPX4 mRNA (Fig. 4I, p < 0.05). Overexpression of YTHDF2 rescued GPX4 mRNA and protein levels and stability in the absence of METTL3 (Fig. 4J, p < 0.05), consequently increasing the GPX4 protein expression (Fig. 4K, **Supplementary Fig.** 13, p < 0.05). Neurons were treated with actinomycin D, and the mRNA level of GPX4 was detected by qPCR assay.

3.5 METTL3 Regulates Ferroptosis in Neurons via GPX4 In Vitro

To determine if *METTL3* influences ferroptosis in TBI-induced neuronal damage through *GPX4* regulation, we conducted further analyses. qPCR and western blot assays revealed that *GPX4* knockdown or erastin treatment did not affect *METTL3* expression in neurons (Fig. 5A,B, **Supplementary Fig. 14**). Notably, the neuronal proliferation enhanced by *METTL3* in the damage model was counteracted by *GPX4* knockdown and erastin treatment (Fig. 5C, p < 0.05). This effect was characterized by significantly increased levels of MDA, Fe²⁺, total iron, and ROS, coupled with decreased SOD levels in the *GPX4* knockdown and erastin groups (Fig. 5D,E).

Additionally, both mRNA and protein levels of GPX4 and SLC7A11 were elevated with *METTL3* overexpression, but this increase was attenuated by *GPX4* knockdown and erastin treatment (Fig. 5F–I, **Supplementary Figs. 14,15**, p < 0.05).

3.6 METTL3 Alleviates Brain Damage and Ferroptosis via GPX4 Regulation In Vivo

We investigated the role of METTL3 in regulating GPX4 during TBI using a mouse model with METTL3 overexpression and treatments with siGPX4 or erastin. MWM test results showed that METTL3 enhanced cognitive function in TBI mice (Fig. 6A), reduced NSS scores (Fig. 6B, p < 0.05), and promoted brain recovery (Fig. 6C). These beneficial effects were counteracted by siGPX4 and erastin treatments. Crystal violet and HE staining revealed fewer dentate gyrus neurons (Fig. 6D) and smaller damaged brain areas (Fig. 6E) in METTL3-treated mice, which were negated by GPX4 depletion and erastin-induced ferroptosis. Additionally, METTL3 ameliorated nuclear pyknosis (Fig. 6F), iron-positive cells (Fig. 6G), cortical neuron degeneration (Fig. 6H), and loss of NeuN-positive neurons (Fig. 6H, Supplementary Fig. 16), effects reversed by siGPX4 and erastin. Furthermore, GPX4 knockdown and erastin increased the production and secretion of inflammatory factors *IL-6*, *TNF-\alpha*, and *IL-1\beta* (Fig. 7A–C, **Sup**plementary Fig. 17, p < 0.05). The METTL3-mediated decrease in Iba-1+ microglia and GFAP+ astrocytes during TBI was also reversed by siGPX4 and erastin (Fig. 7D).

Assessments of ferroptosis biomarkers revealed that *METTL3* mitigated TBI-induced ferroptosis, as evidenced by decreased levels of MDA, Fe^{2+} , total iron, and lipid ROS, coupled with increased SOD levels (Fig. 8A, p < 0.05).

Conversely, si*GPX4* silencing and erastin treatment negated these protective effects. Additionally, si*GPX4* and erastin treatment downregulated the *METTL3*-induced up-



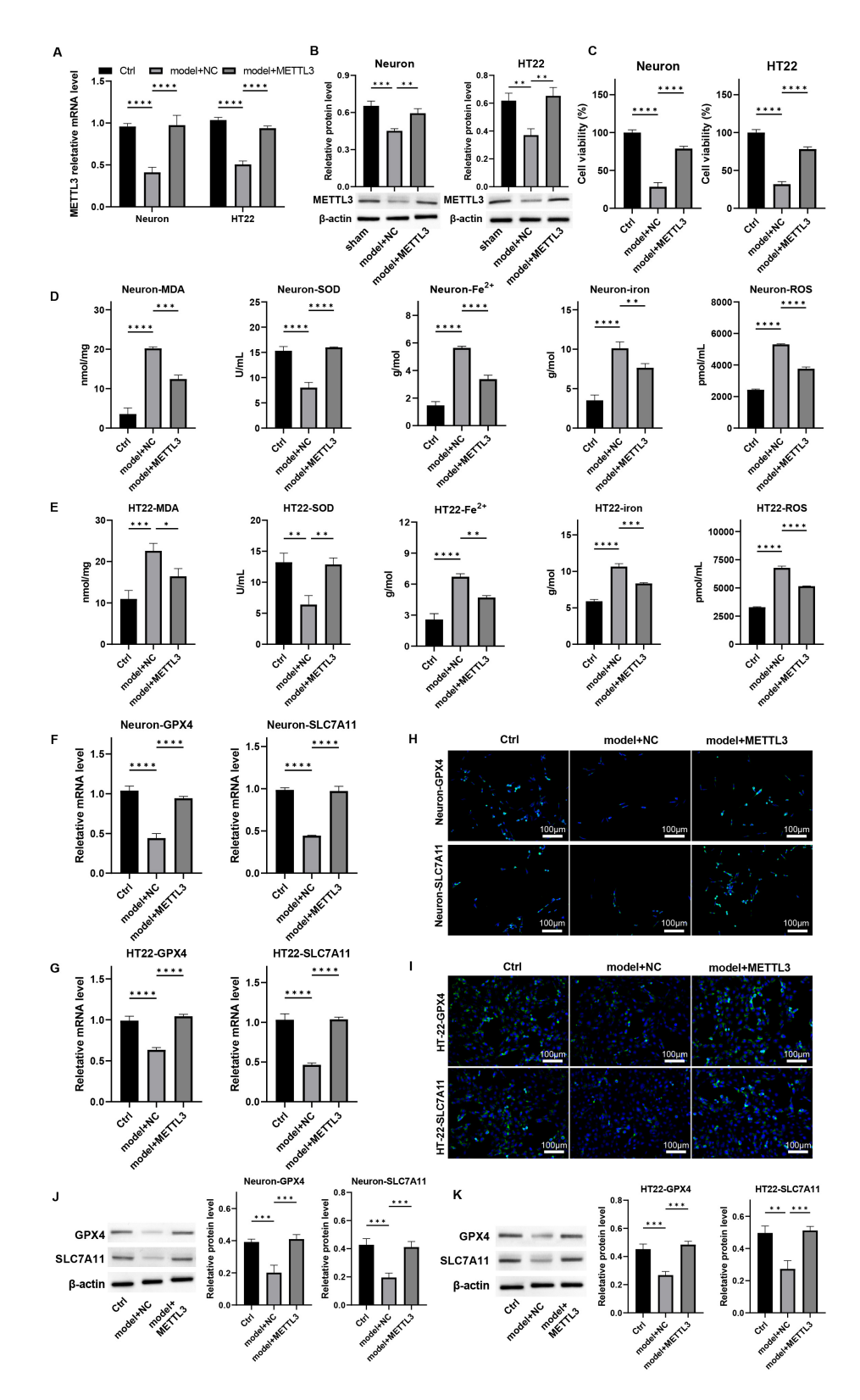


Fig. 3. Overexpression of *METTL3* protects neuron viability and alleviates ferroptosis *in vitro*. Primary neurons and HT-22 cells were processed by mechanical injury and treated with *METTL3* overexpression. The mRNA and protein levels of METTL3 were measured by (A) qPCR and (B) western blot. (C) Cell viability was detected by CCK-8 assay. (D,E) The levels of MDA, SOD, Fe²⁺, total iron, and lipid ROS were measured. (F,G) The mRNA levels of GPX-4 and SLC7A11 in cells were detected by qPCR. (H–K) The protein expression of GPX4 and SLC7A11 in cells was determined by (H,I) immunofluorescence staining, scale bar = 100 μ m, and (J,K) western blot assay. *p < 0.05, **p < 0.01, ****p < 0.001, ****p < 0.0001. n = 3 for each group.

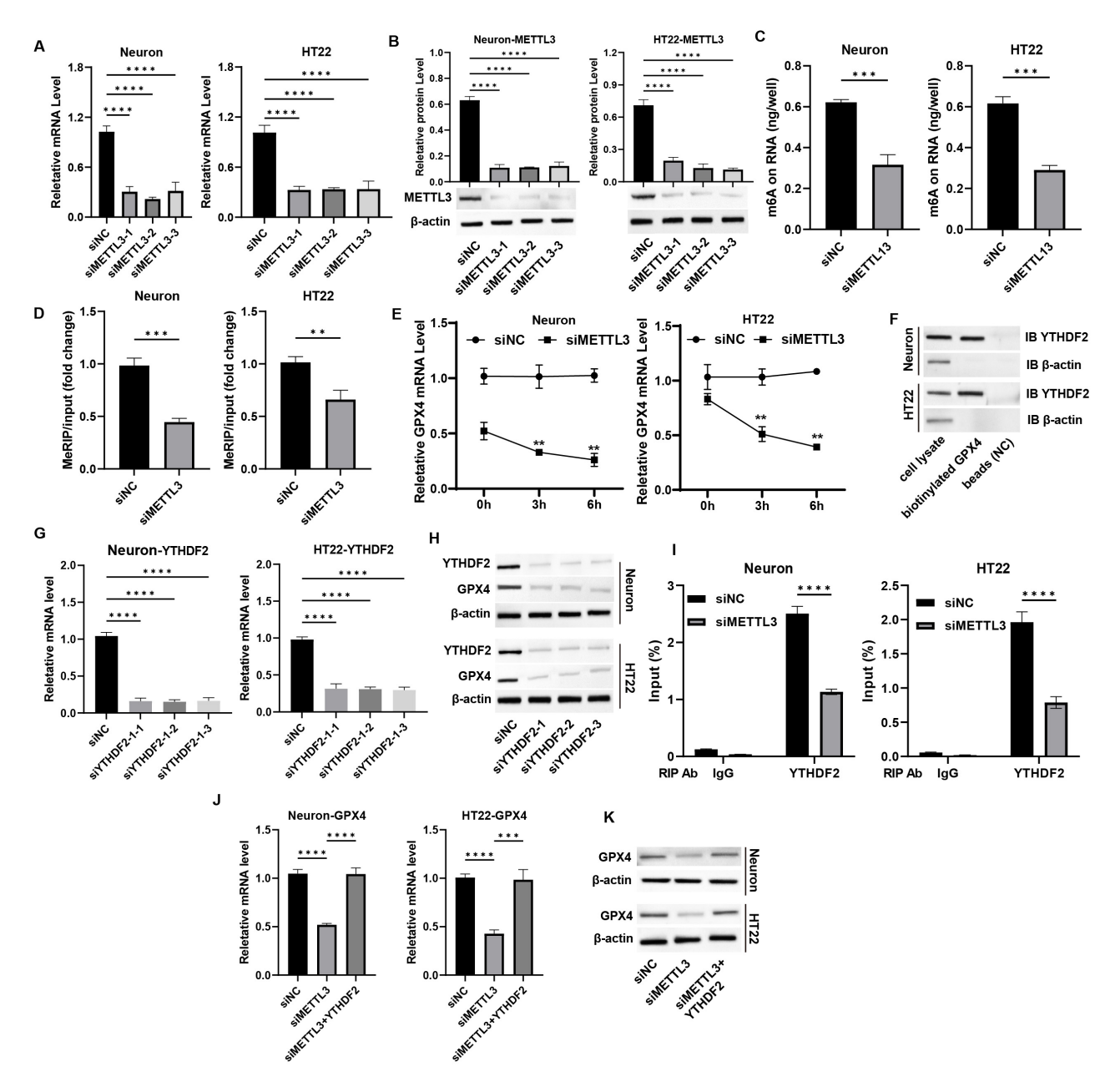


Fig. 4. METTL3 epigenetically regulates GPX4 expression in neurons. (A,B) Neurons were transfected with siMETTL3, and the (A) mRNA and (B) protein levels of METTL3 were measured by qPCR and western blot assay. (C) The total m6A level was measured by m6A-ELISA assay. (D) The m6A enrichment on GPX4 mRNA was detected by MeRIP assay. (E) Neurons were treated with actinomycin D, and the mRNA level of GPX4 was detected by qPCR assay. (F) The interaction between YTHDF2 and GPX4 mRNA was measured by RNA pulldown assay. (G,H) Neurons were transfected with siYTHDF2, and the (G) mRNA and (H) protein levels of YTHDF2 were measured by qPCR and western blot assay. (I) RIP-qPCR assay was performed to measure the binding of YTHDF with GPX4 mRNA. (J) Neurons were transfected with siMETTL3 and YTHDF2 overexpression vectors, and the mRNA level of GPX4 was measured by qPCR assay. (K) The protein level of GPX4 was measured by western blot assay. **p < 0.001, ***p < 0.0001. n = 3 for each group.

regulation of GPX4 and SLC7A11 at mRNA and protein levels (Fig. 8B–D, **Supplementary Figs. 18,19**, p < 0.05). Collectively, these findings indicate that METTL3 exerts neuroprotective effects against TBI by modulating GPX4 expression.

4. Discussion

TBI is recognized as a significant risk factor for neurodegenerative conditions, including Alzheimer's disease and chronic traumatic encephalopathy, and is associated with persistent cognitive deficits [29]. Our study revealed a decrease in *METTL3* levels within the brain tissues of TBI-



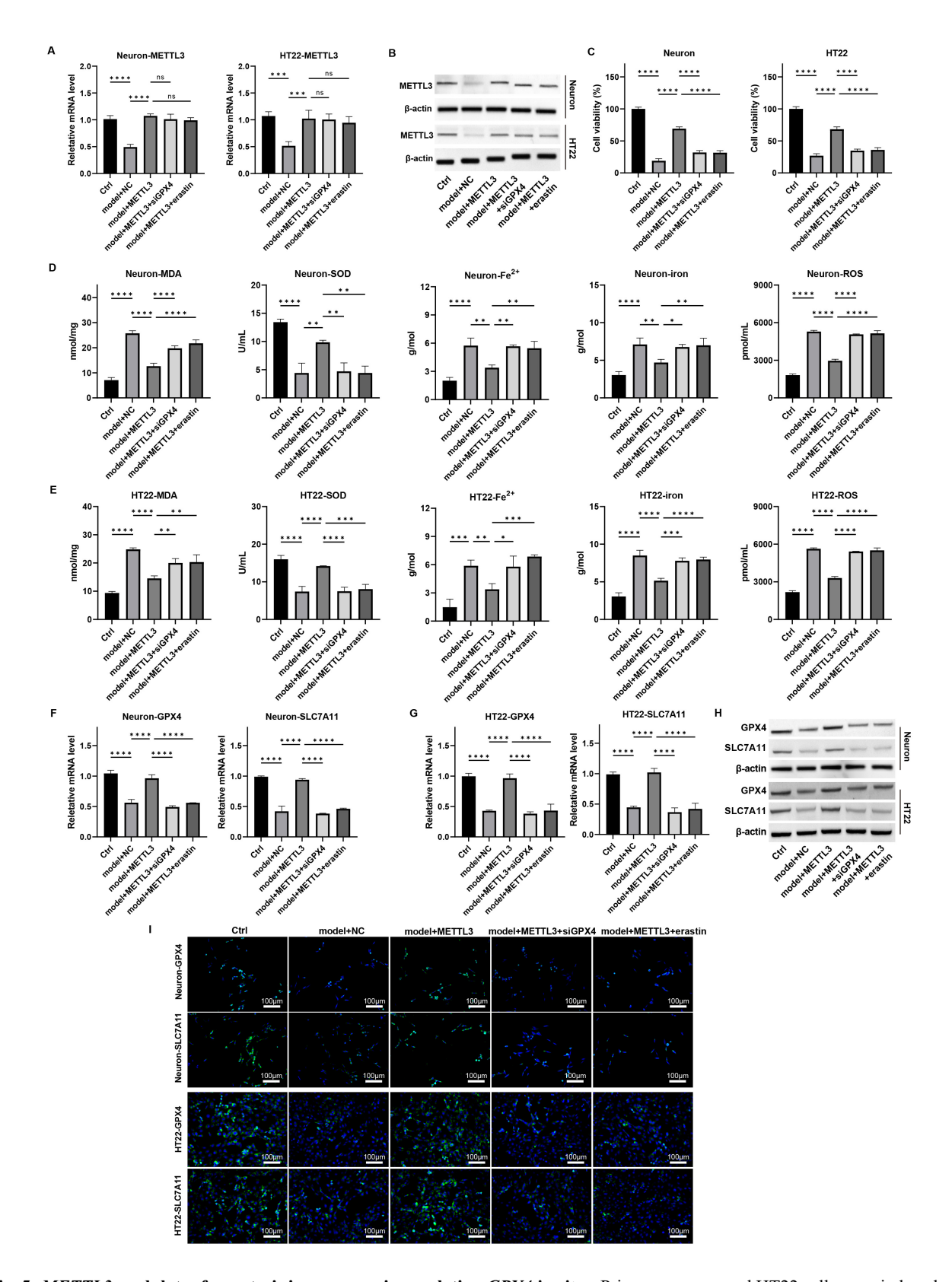


Fig. 5. METTL3 modulates ferroptosis in neurons via regulating GPX4 in vitro. Primary neurons and HT22 cells were induced with mechanical damage and treated with METTL3 overexpression, siGPX4, and erastin. (A,B) The mRNA and protein levels of METTL3 were measured by (A) qPCR and (B) western blot. (C) Cell viability was detected by CCK-8 assay. (D,E) The levels of MDA, SOD, Fe²⁺, total iron, and lipid ROS were measured. (F,G) The mRNA levels of GPX4 and SLC7A11 in cells were detected by qPCR. (H,I) The protein expression of GPX4 and SLC7A11 in cells was determined by (H) western blot and (I) immunofluorescence staining assay. Scale bar = $100 \mu m$, ns: p > 0.05, *p < 0.05, *p < 0.01, ***p < 0.001, ****p < 0.0001. n = 3 for each group.

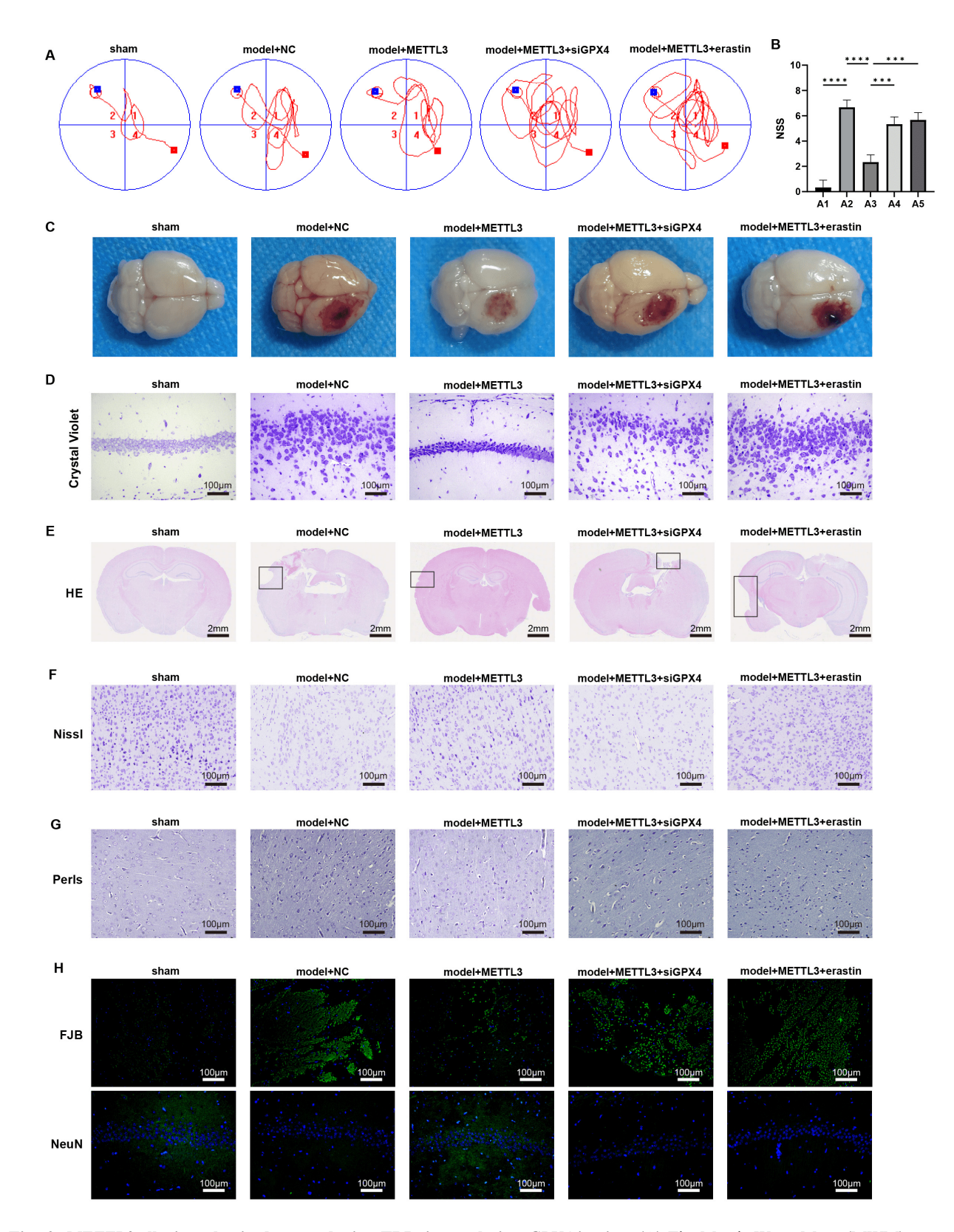


Fig. 6. *METTL3* alleviates brain damage during TBI via regulating *GPX4* in vivo. (A) The Morris Water Maze (MWM) test was performed on day 7 post-TBI. (B) NSS score of brain damage. (C) Representative images of the brain. (D) Crystal violet staining of brain tissues. Scale bar = 100 μ m. (E–H) Representative images of (E) HE, scale bar = 2 mm, (F) Nissl,scale bar = 100 μ m, (G) Perls,scale bar = 100 μ m, (H) Fluoro-Jade B (FJB) and immunofluorescence staining of markers of neuron (NeuN) in brain sections, scale bar = 100 μ m; Cortical contusion areas are represented by rectangles. ***p < 0.001, ****p < 0.0001. A1, sham; A2, model + NC; A3, model + METTL3; A4, model + METTL3 + siGPX4; A5, model + METTL3 + erastin. n = 3 for each group.

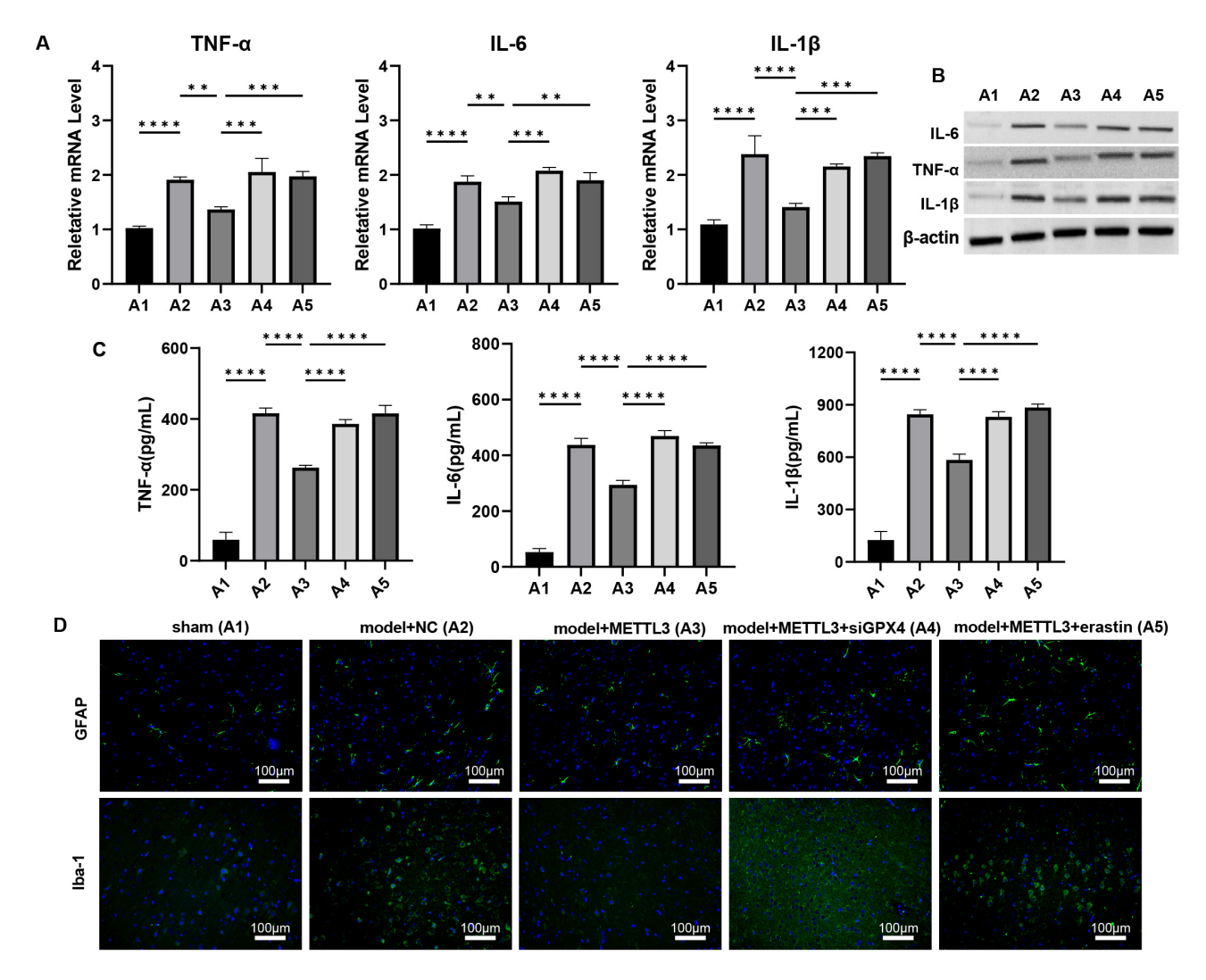


Fig. 7. METTL3 alleviates brain inflammation response during TBI via regulating GPX4 in vivo. (A–C) The mRNA and protein levels of IL-6, TNF- α , and IL-1 β in cortex tissues of TBI mice were measured by (A) qPCR, (B) western blot, and (C) ELISA experiment. (D) Immunofluorescence staining of GFAP and Iba-1. Scale bar = $100 \mu m$, **p < 0.01, ***p < 0.001, ****p < 0.0001. A1, sham; A2, model + NC; A3, model + METTL3; A4, model + METTL3 + siGPX4; A5, model + METTL3 + erastin. n = 3 for each group.

afflicted mice. The enhancement of *METTL3* expression significantly mitigated cognitive impairments triggered by TBI, reduced brain lesion severity, diminished neuronal damage, and regulated iron accumulation in brain tissue. These observations suggest that *METTL3* may play a neuroprotective role against TBI-induced injuries, fostering the repair and recovery of brain tissue as well as cognitive functions.

Neuroinflammation is a pivotal secondary injury mechanism following TBI, with the activation of microglia and astrocytes playing a crucial role [30,31]. As the primary immune cells of the central nervous system, microglia are swiftly activated upon TBI, modulating inflammatory responses through morphological changes and cytokine release [32]. These activated microglia can manifest either pro-inflammatory or anti-inflammatory phenotypes. Specifically, the M1 subtype, characterized by classical ac-

tivation, secretes pro-inflammatory cytokines like $TNF-\alpha$ and $IL-1\beta$, potentially aggravating brain injury [33]. Our findings indicate that METTL3 overexpression curbs the production of inflammatory mediators and inhibits the activation of Iba-1+ microglia and GFAP+ astrocytes, suggesting that METTL3 attenuates neuroinflammation post-TBI.

Lipid peroxidation, catalyzed by iron, is a hallmark of ferroptosis [34]. Our study suggests that *METTL3* may offer neuroprotection by mitigating the buildup of lipid ROS and iron (Fe²⁺) within neurons in both cellular and animal models of TBI. Furthermore, *METTL3* modulates the expression of critical genes *GPX4* and *SLC7A11*, hinting at a mechanism of action that likely involves the inhibition of ferroptosis. Ferroptosis is characterized by iron accumulation, extensive lipid peroxidation, weakened antioxidant defenses, and increased ROS production, all of which are intimately linked to oxidative stress and the pathogenesis of



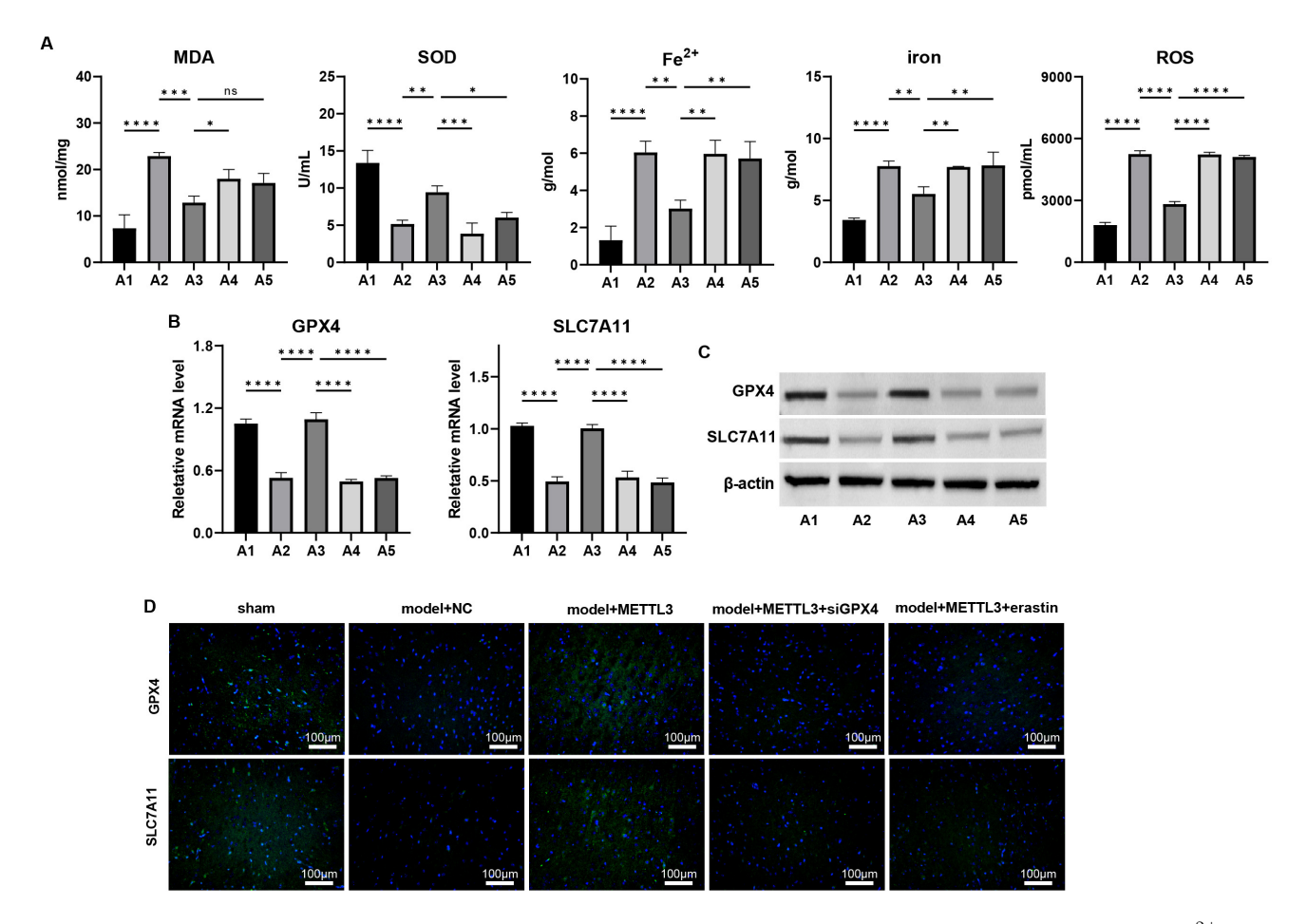


Fig. 8. METTL3 alleviates ferroptosis during TBI via regulating GPX4 in vivo. (A) The cortical levels of MDA, SOD, Fe²⁺, total iron, and lipid ROS were measured. (B–D) The mRNA and protein levels of GPX4 and SLC7A11 in cortex tissues of TBI mice were measured by (B) qPCR, (C) western blot, and (D) immunofluorescence staining. Scale bar = 100 μ m, ns: p > 0.05, *p < 0.05, **p < 0.01, ****p < 0.001, ****p < 0.0001. n = 3 for each group.

neurological disorders and brain injuries [12,13]. Consistent with previous research [12,35], our study verified that TBI causes iron homeostasis disruptions and elevated lipid ROS levels, both indicative of ferroptosis. These findings support the notion that ferroptosis substantially contributes to TBI pathophysiology. *METTL3* seems to counter these effects, suggesting its potential as a protective agent against the ferroptosis phenotype linked to TBI.

The N6-methyladenosine (m6A) modification is the prevalent mRNA modification in eukaryotes [36]. This mRNA modification is dynamic and reversible, regulated by proteins categorized as "writers"—including METTL3—"erasers" such as FTO and ALKBH5, and "readers" comprising YTH domain-containing proteins like YTHDF1-3 and YTHDC1-2 [37,38]. These reader proteins identify m6A sites on RNA, influencing RNA processing aspects such as stability, degradation, splicing, and translation. METTL3, a key to the m6A methyltransferase complex, regulates gene expression via this modification. Notably, METTL3's irregular expression has been linked to various cancers [39], implying a connection between m6A

modification and carcinogenesis. However, the mechanisms underlying *METTL3* dysregulation in TBI remain obscure. Our study reveals that *YTHDF2* directly interacts with *GPX4* mRNA, serving as a reader protein that enhances m6A modification and RNA stability on *GPX4* mRNA. Modulating *METTL3* levels or activity could potentially alleviate cognitive deficits, curb neuroinflammation, and shield neurons from ferroptosis-induced damage. Further research is essential to clarify the neuroprotective mechanisms of *METTL3* and to assess the therapeutic potential of targeting the m6A pathway in TBI and other neurological disorders.

5. Conclusion

Our findings demonstrate that *METTL3* exerts a protective influence against TBI-induced neurological deficits, lesion volume, and neurodegeneration by suppressing ferroptosis. *METTL3*'s anti-ferroptosis properties likely facilitate functional recovery post-TBI through the regulation of m6A modification and RNA stability of *GPX4*. This study advances our understanding of how *METTL3*-mediated epi-



genetic modifications relate to TBI-induced brain damage, indicating *METTL3*'s potential as a therapeutic target for TBI. Addressing the limitations and challenges identified will be crucial for the translation of *METTL3*-based therapies into clinical practice.

Availability of Data and Materials

The datasets used and analyzed during the current study are available from the corresponding author on reasonable request.

Author Contributions

FQ, FL and XY designed the research study. FQ, WZ and FL performed the research. SZ and JS analyzed the data. All authors contributed to editorial changes in the manuscript. All authors read and approved the final manuscript. All authors have participated sufficiently in the work and agreed to be accountable for all aspects of the work

Ethics Approval and Consent to Participate

All animal experiments were conducted in strict accordance with the ethical guidelines and regulations established by the Animal Ethics Committee of Medical Discovery Leader (MDL). The study protocol was reviewed and approved by the committee under approval number MDL2023-08-26-01.

Acknowledgment

Not applicable.

Funding

This research received no external funding.

Conflict of Interest

The authors declare no conflict of interest.

Supplementary Material

Supplementary material associated with this article can be found, in the online version, at https://doi.org/10.31083/FBL31304.

References

- Capizzi A, Woo J, Verduzco-Gutierrez M. Traumatic Brain Injury: An Overview of Epidemiology, Pathophysiology, and Medical Management. The Medical Clinics of North America. 2020; 104: 213–238. https://doi.org/10.1016/j.mcna.2019.11.001
- [2] Kochanek PM, Tasker RC, Carney N, Totten AM, Adelson PD, Selden NR, et al. Guidelines for the Management of Pediatric Severe Traumatic Brain Injury, Third Edition: Update of the Brain Trauma Foundation Guidelines, Executive Summary. Neurosurgery. 2019; 84: 1169–1178. https://doi.org/10.1093/neuros/nyz051.
- [3] Hu X, Zhang H, Zhang Q, Yao X, Ni W, Zhou K. Emerging role of STING signalling in CNS injury: inflammation,

- autophagy, necroptosis, ferroptosis and pyroptosis. Journal of Neuroinflammation. 2022; 19: 242. https://doi.org/10.1186/s12974-022-02602-y.
- [4] Nie Z, Tan L, Niu J, Wang B. The role of regulatory necrosis in traumatic brain injury. Frontiers in Molecular Neuroscience. 2022; 15: 1005422. https://doi.org/10.3389/fnmol. 2022.1005422.
- [5] Chen X, Ning Y, Wang B, Qin J, Li C, Gao R, et al. HET0016 inhibits neuronal pyroptosis in the immature brain post-TBI via the p38 MAPK signaling pathway. Neuropharmacology. 2023; 239: 109687. https://doi.org/10.1016/j.neuropharm.2023.109687.
- [6] Zeng F, Nijiati S, Tang L, Ye J, Zhou Z, Chen X. Ferroptosis Detection: From Approaches to Applications. Angewandte Chemie. 2023; 62: e202300379. https://doi.org/10.1002/anie.202300379.
- [7] Jiang X, Stockwell BR, Conrad M. Ferroptosis: mechanisms, biology and role in disease. Nature Reviews. Molecular Cell Biology. 2021; 22: 266–282. https://doi.org/10.1038/s41580-020-00324-8.
- [8] Mahoney-Sánchez L, Bouchaoui H, Ayton S, Devos D, Duce JA, Devedjian JC. Ferroptosis and its potential role in the physiopathology of Parkinson's Disease. Progress in Neurobiology. 2021; 196: 101890. https://doi.org/10.1016/j.pneurobio.2020. 101890.
- [9] Wu X, Li Y, Zhang S, Zhou X. Ferroptosis as a novel therapeutic target for cardiovascular disease. Theranostics. 2021; 11: 3052– 3059. https://doi.org/10.7150/thno.54113.
- [10] Li J, Cao F, Yin HL, Huang ZJ, Lin ZT, Mao N, et al. Ferroptosis: past, present and future. Cell Death & Disease. 2020; 11: 88. https://doi.org/10.1038/s41419-020-2298-2.
- [11] Cheng Y, Gao Y, Li J, Rui T, Li Q, Chen H, et al. TrkB agonist N-acetyl serotonin promotes functional recovery after traumatic brain injury by suppressing ferroptosis via the PI3K/Akt/Nrf2/Ferritin H pathway. Free Radical Biology & Medicine. 2023; 194: 184–198. https://doi.org/10.1016/j.freeradbiomed.2022.12.002.
- [12] Rui T, Wang H, Li Q, Cheng Y, Gao Y, Fang X, et al. Deletion of ferritin H in neurons counteracts the protective effect of melatonin against traumatic brain injury-induced ferroptosis. Journal of Pineal Research. 2021; 70: e12704. https://doi.org/10.1111/ jpi.12704.
- [13] Xie BS, Wang YQ, Lin Y, Mao Q, Feng JF, Gao GY, et al. Inhibition of ferroptosis attenuates tissue damage and improves long-term outcomes after traumatic brain injury in mice. CNS Neuroscience & Therapeutics. 2019; 25: 465–475. https://doi.org/10.1111/cns.13069.
- [14] Britt EC, John SV, Locasale JW, Fan J. Metabolic regulation of epigenetic remodeling in immune cells. Current Opinion in Biotechnology. 2020; 63: 111–117. https://doi.org/10.1016/j.co pbio.2019.12.008.
- [15] Hogg SJ, Beavis PA, Dawson MA, Johnstone RW. Targeting the epigenetic regulation of antitumour immunity. Nature Reviews. Drug Discovery. 2020; 19: 776–800. https://doi.org/10. 1038/s41573-020-0077-5.
- [16] Miranda Furtado CL, Dos Santos Luciano MC, Silva Santos RD, Furtado GP, Moraes MO, Pessoa C. Epidrugs: targeting epigenetic marks in cancer treatment. Epigenetics. 2019; 14: 1164– 1176. https://doi.org/10.1080/15592294.2019.1640546.
- [17] Orsolic I, Carrier A, Esteller M. Genetic and epigenetic defects of the RNA modification machinery in cancer. Trends in Genetics: TIG. 2023; 39: 74–88. https://doi.org/10.1016/j.tig.2022. 10.004
- [18] Huang W, Chen TQ, Fang K, Zeng ZC, Ye H, Chen YQ. N6-methyladenosine methyltransferases: functions, regulation, and clinical potential. Journal of Hematology & Oncology. 2021; 14: 117. https://doi.org/10.1186/s13045-021-01129-8.



- [19] Sendinc E, Shi Y. RNA m6A methylation across the transcriptome. Molecular Cell. 2023; 83: 428–441. https://doi.org/10.1016/j.molcel.2023.01.006.
- [20] Chai RC, Chang YZ, Chang X, Pang B, An SY, Zhang KN, et al. YTHDF2 facilitates UBXN1 mRNA decay by recognizing METTL3-mediated m⁶A modification to activate NF-κB and promote the malignant progression of glioma. Journal of Hematology & Oncology. 2021; 14: 109. https://doi.org/10.1186/s13045-021-01124-z.
- [21] Chen M, Wei L, Law CT, Tsang FHC, Shen J, Cheng CLH, et al. RNA N6-methyladenosine methyltransferase-like 3 promotes liver cancer progression through YTHDF2-dependent posttranscriptional silencing of SOCS2. Hepatology. 2018; 67: 2254– 2270. https://doi.org/10.1002/hep.29683.
- [22] Meng X, Wang Z, Yang Q, Liu Y, Gao Y, Chen H, et al. Intracellular C5aR1 inhibits ferroptosis in glioblastoma through METTL3-dependent m6A methylation of GPX4. Cell Death & Disease. 2024; 15: 729. https://doi.org/10.1038/s41419-024-06963-5.
- [23] Lin L, Hu X, Li Q, Huang L. Methyltransferase-like 3 (METTL3) Epigenetically Modulates Glutathione Peroxidase 4 (GPX4) Expression to Affect Asthma. Iranian Journal of Allergy, Asthma, and Immunology. 2023; 22: 551–560. https://doi.org/10.18502/ijaai.v22i6.14644.
- [24] Li N, Yi X, He Y, Huo B, Chen Y, Zhang Z, *et al.* Targeting Ferroptosis as a Novel Approach to Alleviate Aortic Dissection. International Journal of Biological Sciences. 2022; 18: 4118–4134. https://doi.org/10.7150/ijbs.72528.
- [25] Wu X, Liu H, Wang J, Zhang S, Hu Q, Wang T, et al. The m⁶A methyltransferase METTL3 drives neuroinflammation and neurotoxicity through stabilizing BATF mRNA in microglia. Cell Death and Differentiation. 2025; 32: 100–117. https://doi.org/10.1038/s41418-024-01329-y.
- [26] Osier N, Dixon CE. Controlled cortical impact for modeling traumatic brain injury in animals. In Srivastava A, Cox C, (eds.) Pre-Clinical and Clinical Methods in Brain Trauma Research (pp. 81–95). Humana Press: New York, NY. 2018. https://doi.org/10.1007/978-1-4939-8564-7 5.
- [27] Koton S, Patole S, Carlson JM, Haight T, Johansen M, Schneider ALC, et al. Methods for stroke severity assessment by chart review in the Atherosclerosis Risk in Communities study. Scientific Reports. 2022; 12: 12338. https://doi.org/10.1038/s41598-022-16522-7.
- [28] Weng W, He Z, Ma Z, Huang J, Han Y, Feng Q, *et al*. Tufm lactylation regulates neuronal apoptosis by modulating mitophagy in traumatic brain injury. Cell Death and Differentiation. 2025; 32: 530–545. https://doi.org/10.1038/s41418-024-01408-0.

- [29] McAllister TW. Neurobehavioral sequelae of traumatic brain injury: evaluation and management. World Psychiatry. 2008; 7: 3–10. https://doi.org/10.1002/j.2051-5545.2008.tb00139.x.
- [30] Kalra S, Malik R, Singh G, Bhatia S, Al-Harrasi A, Mohan S, et al. Pathogenesis and management of traumatic brain injury (TBI): role of neuroinflammation and anti-inflammatory drugs. Inflammopharmacology. 2022; 30: 1153–1166. https://doi.org/10.1007/s10787-022-01017-8.
- [31] Shi G, Liu L, Cao Y, Ma G, Zhu Y, Xu J, et al. Inhibition of neutrophil extracellular trap formation ameliorates neuroinflammation and neuronal apoptosis via STING-dependent IRE1α/ASK1/JNK signaling pathway in mice with traumatic brain injury. Journal of Neuroinflammation. 2023; 20: 222. https://doi.org/10.1186/s12974-023-02903-w.
- [32] Hegdekar N, Sarkar C, Bustos S, Ritzel RM, Hanscom M, Ravishankar P, et al. Inhibition of autophagy in microglia and macrophages exacerbates innate immune responses and worsens brain injury outcomes. Autophagy. 2023; 19: 2026–2044. https://doi.org/10.1080/15548627.2023.2167689.
- [33] Wû H, Zheng J, Xu S, Fang Y, Wu Y, Zeng J, et al. Mer regulates microglial/macrophage M1/M2 polarization and alleviates neuroinflammation following traumatic brain injury. Journal of Neuroinflammation. 2021; 18: 2. https://doi.org/10.1186/s12974-020-02041-7.
- [34] Hirschhorn T, Stockwell BR. The development of the concept of ferroptosis. Free Radical Biology & Medicine. 2019; 133: 130– 143. https://doi.org/10.1016/j.freeradbiomed.2018.09.043.
- [35] Cheng Y, Qu W, Li J, Jia B, Song Y, Wang L, et al. Ferristatin II, an Iron Uptake Inhibitor, Exerts Neuroprotection against Traumatic Brain Injury via Suppressing Ferroptosis. ACS Chemical Neuroscience. 2022; 13: 664–675. https://doi.org/10.1021/acsc hemneuro.1c00819.
- [36] Meyer KD, Saletore Y, Zumbo P, Elemento O, Mason CE, Jaffrey SR. Comprehensive analysis of mRNA methylation reveals enrichment in 3' UTRs and near stop codons. Cell. 2012; 149: 1635–1646. https://doi.org/10.1016/j.cell.2012.05.003.
- [37] Wang X, Lu Z, Gomez A, Hon GC, Yue Y, Han D, et al. N6-methyladenosine-dependent regulation of messenger RNA stability. Nature. 2014; 505: 117–120. https://doi.org/10.1038/nature12730.
- [38] He L, Li H, Wu A, Peng Y, Shu G, Yin G. Functions of N6-methyladenosine and its role in cancer. Molecular Cancer. 2019; 18: 176. https://doi.org/10.1186/s12943-019-1109-9.
- [39] Zeng C, Huang W, Li Y, Weng H. Roles of METTL3 in cancer: mechanisms and therapeutic targeting. Journal of Hematology & Oncology. 2020; 13: 117. https://doi.org/10.1186/s13045-020-00951-w.

